ELSEVIER

Contents lists available at ScienceDirect

Journal of Chemical Neuroanatomy

journal homepage: www.elsevier.com/locate/jchemneu



Automatic ground truth for deep learning stereology of immunostained neurons and microglia in mouse neocortex



Hady Ahmady Phoulady^{a,*}, Dmitry Goldgof^b, Lawrence O. Hall^b, Peter R. Mouton^{b,c}

- a Department of Computer Science, University of Southern Maine, Portland, ME, USA
- ^b Department of Computer Science and Engineering, University of South Florida, Tampa, FL, USA
- c SRC Biosciences, Tampa, FL, USA

ARTICLE INFO

Keywords:
Stereology
Cell counting
Neuron
Microglia
Segmentation
Manual ground truth
Gold standard
Neural network
Optical fractionator

ABSTRACT

Collection of unbiased stereology data currently relies on relatively simple, low throughput technology developed in the mid-1990s. In an effort to improve the accuracy and efficiency of these integrated hardware-software-digital microscopy systems, we have developed an automatic segmentation algorithm (ASA) for automatic stereology counts using the unbiased optical fractionator method. Here we report on a series of validation experiments in which immunostained neurons (NeuN) and microglia (Iba1) were automatically counted in tissue sections through a mouse neocortex. In the first step, a minimum of 100 systematic-random z-axis image stacks (disector stacks) containing NeuN- and Iba1-immunostained cells were automatically collected using a softwarecontrolled 3 axes (XYZ) stage motor. In the second step, each disector stack was converted to an extended depth of field (EDF) image in which each cell is shown at its optimal plane of focus. Third, individual neurons and microglia were segmented and the regional minimas were extracted and used as seed regions for cells in a watershed segmentation algorithm. Finally, the unbiased disector frame and counting rules were used to make unbiased parameter estimates for neurons and microglia cells. The results for both NeuN neurons and Iba1 microglia were compared to manual counts made by a moderately experienced data collector from the same disector stacks. The final results show lower error rates for counts of Iba1-immunostained microglia cells than for quantifying NeuN-immunostained neurons, most likely due to less three-dimensional overlapping of Iba1 cells. We report that the throughput efficiency of using ASA to automatically annotate images of Iba1 microglia is more than five times greater than that of manual stereology counts of the same sections. Moreover, we show that ASA is significantly more accurate in counting microglia cells than a moderately experienced data collector (about 10% higher overall accuracy) when both were compared to counts by an expert neurohistologist. Thus, the ASA method applied to EDF images from disector stacks can be extremely useful to automate and increase the accuracy of cell counts, which could be especially helpful and cost-effective when expert help is not available. Another potential use of our ASA approach is to generate unsupervised ground truth as an efficient alternative to manual annotation for training deep learning models, as shown in our ongoing work.

1. Introduction

Digital anatomy and pathology refer to the study of healthy and diseased tissue, respectively, from digitized images of microscopic biologic structures such as cells, fibers, and blood vessels. Unbiased (design-based) stereology is the state-of-the-art method for quantifying brain cells (neurons, microglia) in basic neuroscience research and drug discovery studies involving neurodegeneration and neuroinflammation. A major weakness of these theoretically powerful stereology methods is the continuing dependence on low throughput technology that requires subjective manual counting (clicks) by highly trained technicians.

These computer-assisted manual stereology studies suffer from high labor costs, error-prone data collection, user subjectivity and fatigue. Here we report on our continuing efforts to improve the accuracy, precision and efficiency of these processes by incorporating a series of recently developed machine learning techniques to support fully automatic stereology analyses of high signal:noise (S:N) stained cells on tissue sections.

2. Related work

A large and growing number of reviewers for peer-review journals

E-mail address: parham.ap@gmail.com (H. Ahmady Phoulady).

^{*} Corresponding author.

and funding agencies now prefer stereology data to less accurate (methodologically biased) morphometric and image analysis methods (Saper, 1996; Mouton, 2002, 2011). To improve throughput of these studies over manual counts by highly trained data collectors, we developed an automated approach and show that machine learning can be used for accurate and efficient stereology of biological tissue. As in the case of manual stereology of immunostained cells, machine learning can overcome common sources of stereology bias (e.g., corpuscle problem, faulty correction factors, the reference trap) to generate stereology data using theoretically unbiased methods.

For instance, our previous work shows that an adaptive segmentation algorithm (ASA) can make unbiased counts of NeuN-immunostained neurons with greater accuracy, precision and efficiency than manual stereology counts of the same sections (Mouton et al., 2017). The present study expands this work to show that with only minor modifications the same ASA approach can achieve similar performance for stereology counts of microglia equivalent to that of a moderately experienced data collector in about one-fifth the time they take. Typically, data will be collected by moderately experienced people due to the cost of an expert for the long collection times. Importantly, both methods use the same hardware configuration consisting of a microscope equipped with low-to-high resolution lenses and motorized XYZ stage; moderate resolution digital camera; and standard computer/monitor. Besides the benefit of higher throughput, automatic stereology reduces inter-rater variability due to user errors, subjectivity and fatigue.

To date, our applications of automatic stereology have focused on the total number and density of NeuN neurons on tissue sections. Here, we show that the same ASA approach with only minor modifications can be used for unbiased stereology counts of another important population of brain cells, i.e., Iba1-immunopositive microglia cells, which are critical for a wide range of neuroinflammation studies. Finally, the ASA approach can dramatically reduce the work-effort by a human data collector to create ground truth (image annotations) when training a convolutional neural network (CNN) model to do segmentation using deep learning. Building a relatively large and reliable segmentation dataset (ground truth) is a prerequisite for training a deep neural network to achieve robust results such as shown by Alahmari et al. (2019). Thus, three novel contributions in this work arise from an ASA method that is generalizable for different domains of immunostained tissue sections: (1) automatic counting of both microglia cells (Iba1) and neurons (NeuN) on immunostained tissue sections; (2) more accurate results for stereological quantification of immunostained cells on tissue sections in less than 20% of the time required for manual counts approaches; and (3) automatic creation of the ground truth for more accurate and robust deep learning applications.

3. Materials and methods

Animal handling and use was approved by the USF Institutional Animal Care and Use Committee and followed NIH guidelines for the care and use of laboratory animals. These studies to validate the automatic framework for counting NeuN- and Iba1-immunostained neurons and microglia cells, respectively, used the well-characterized Tg4510 line with responder and activator transgenes that drive expression of a P301L tau mutation under control of a tetracycline operon-responsive element (Santacruz et al., 2005). Tg4510 mice express mutant tau that leads to progressive cognitive decline in parallel with neuron loss and activation of neuroglia cells. Age- and sex-matched non-tg littermate control mice were included to test the automatic framework on normal (non-degenerating) neurons. Rather than test specific hypotheses related to tauopathies, neurodegeneration or neuroinflammation, these genetically modified mice and controls were selected to show a wide range of normal, neurodegenerative and neuroinflammatory phenotypes under brightfield illumination.

3.1. Immunostaining

Sections were placed in a multi-sample staining tray and endogenous peroxidase was blocked (10% methanol, 3% $\rm H_2O_2$ in PBS; 30 min). Mouse sections were permeabilized with 0.2% lysine, 1% Triton X-100 in PBS solution and incubated overnight in anti-NeuN or Iba-1 primary anti-rabbit antibodies from Millipore Sigma and Wako, respectively, at 1:1000 dilution. Sections were washed in PBS, and then incubated in biotinylated secondary antibody (Vector Laboratories, Burlingame, CA). The tissue was again washed after 2 h and incubated with Vectastain* Elite* ABC kit (Vector Laboratories, Burlingame, CA) for enzyme conjugation. Finally, sections were stained using 0.05% diaminobenzidine in 0.03% $\rm H_2O_2$ with nickel intensification. Tissue sections were mounted onto slides, dehydrated, and cover slipped.

3.2. Dataset

The datasets for automatic stereology were collected in conjunction with manual stereology counts of NeuN neurons and Iba1 microglia done at the same systematic-random x–y locations across 6–8 sections through the entire neocortex for six cases (M-1 through M-6). Both the automatic and manual stereology methods were based on unbiased estimation of total cell numbers using the optical fractionator method (West et al., 1991). At each X–Y location, the user collected disector stacks of images consisting of 10 one-mm images in the z-axis (disector height = 10 μ m). Each disector stack was converted into a single synthetic Extended Depth of Field (EDF) image using the algorithm in Bradley and Bamford (2004). The algorithm was applied to over 1300 disector stacks from NeuN-stained cells (neurons) and Iba1 (microglia cells) from brains of six mice (Fig. 1). Each EDF algorithm shows all cells within the disector stack at their optimal (most in focus) plane on a single image (EDF image).

3.3. Segmentation methods

The ASA method proposed here is a newer version of the work in Mouton et al. (2017) along with further experiments on new NeuNstained cases and then modifying and applying the algorithm for counting Iba1-immunostained microglia cells. Since neurons and microglia appear in different shapes and brightness, no a priori shapes can be assumed for the purpose of segmentation. Due to brightness variation at both the image and cell levels, any intensity thresholds used during segmentation must be set in an adaptive and automatic manner. The segmentation pipeline for the ASA is a combination of Gaussian Mixture Model (GMM), morphological operations, watershed segmentation, Voronoi diagrams and boundary smoothing. Each of these steps are illustrated in Fig. 2 as outlined in the legend and detailed below. Creating EDF images is useful to make it possible to process a single image that has every cell in focus automatically rather than looking for in focus cells manually in a Z-stack (volume). For instance, for neurons, Fig. 2(a) shows the image used for the manual counts and Fig. 2(b) is the EDF image. The inclusion line (green) and exclusion lines (red) lines in Fig. 2(i) are for avoiding bias due to edge effects (Gundersen, 1977).

3.3.1. Clump segmentation

Similar to the second step of the algorithm in Ahmady Phoulady et al. (2017), clumps of neurons in the image were segmented as follows. A GMM with two components was estimated based on pixel intensities using the expectation maximization (EM) algorithm. The image was binarized using the threshold computed by a background Gaussian quantile function value (at q=0.06 in this study) minus an offset f. Subsequently, morphological operations were applied to extract the separate clumped cells regions (Fig. 2(c)). Finally, clumps with area smaller than a pre-determined size, c_A , were removed. Because the GMM is estimated by pixel intensities of each image separately it makes the whole framework relatively resistant to brightness variation (see

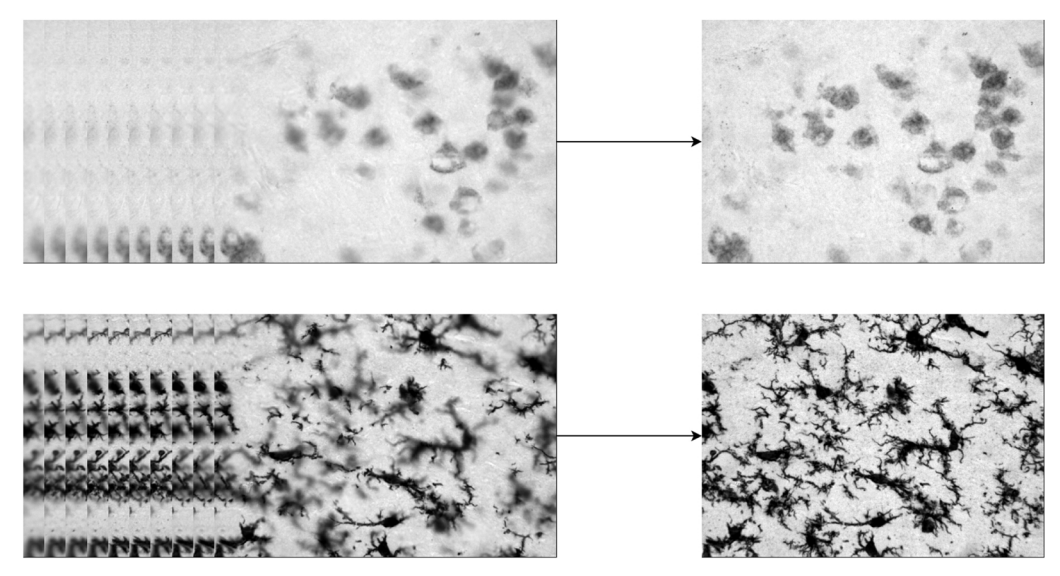


Fig. 1. EDF images of NeuN neurons (upper) and Iba1 microglia (lower) created from z-axis image stacks (left upper and lower) at high power (100 × oil, n.a. 1.4).

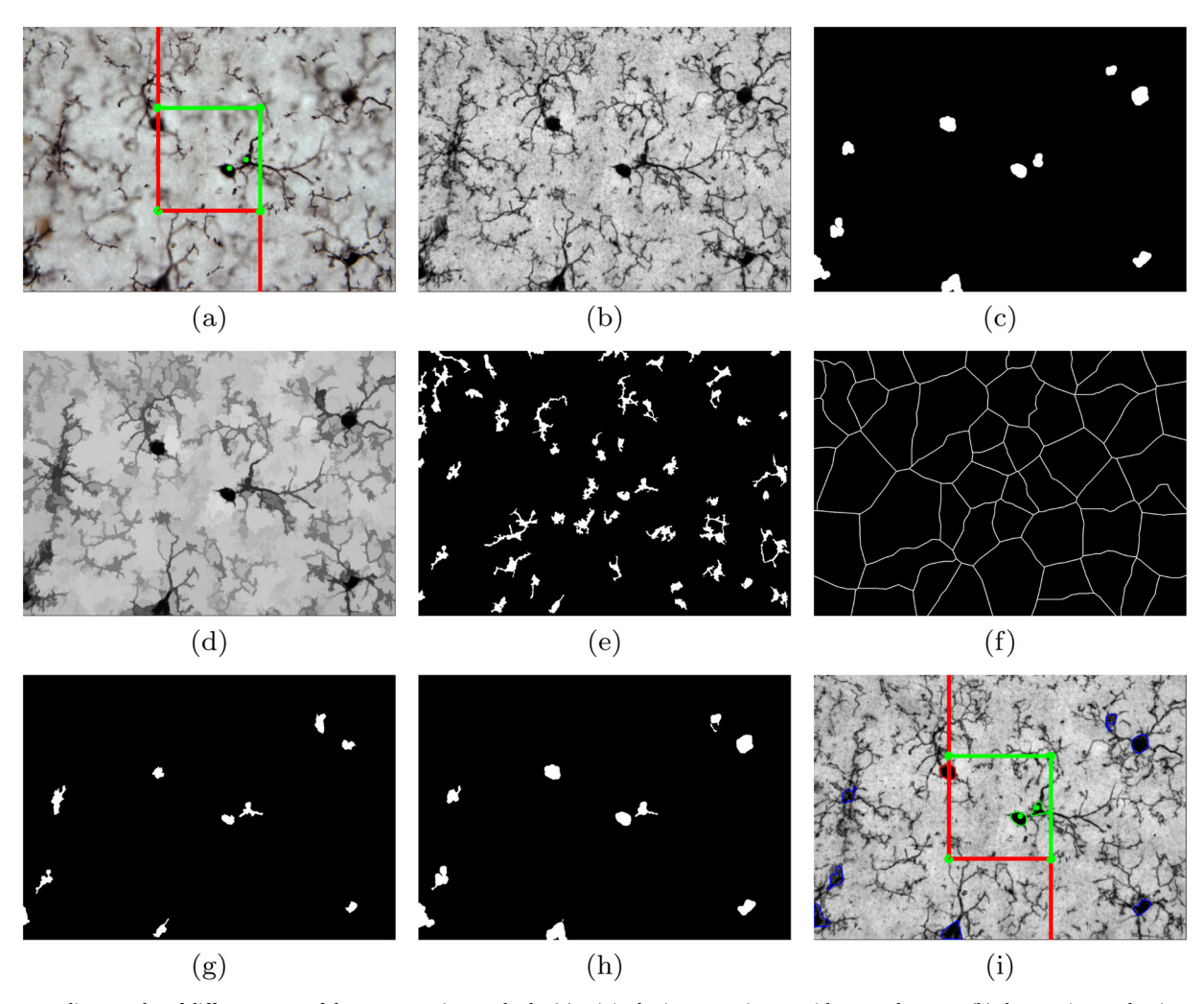


Fig. 2. Intermediate results of different steps of the segmentation methods: (a) original microscopy image with manual counts, (b) the EDF image that is used by the segmentation method, (c) segmented clumps after thresholding the EDF image, (d) processed EDF image, (e) regional minimas in the processed image, (f) providing boundaries (background marker) for watershed segmentation that indicate pixels that do not belong to any cell, (g) watershed segmentation regions reconstructed by regional minimas, (h) expanded foreground regions within each segmented clump boundary, (i) the final segmentation after smoothing region boundaries. Blue regions are segmented regions that do not overlap with the disector frame and therefore are not used for automated counting; red regions are segmented regions that were excluded due to overlap with the exclusion line; and green regions are segmented regions representing microglia cells used for automated counting.

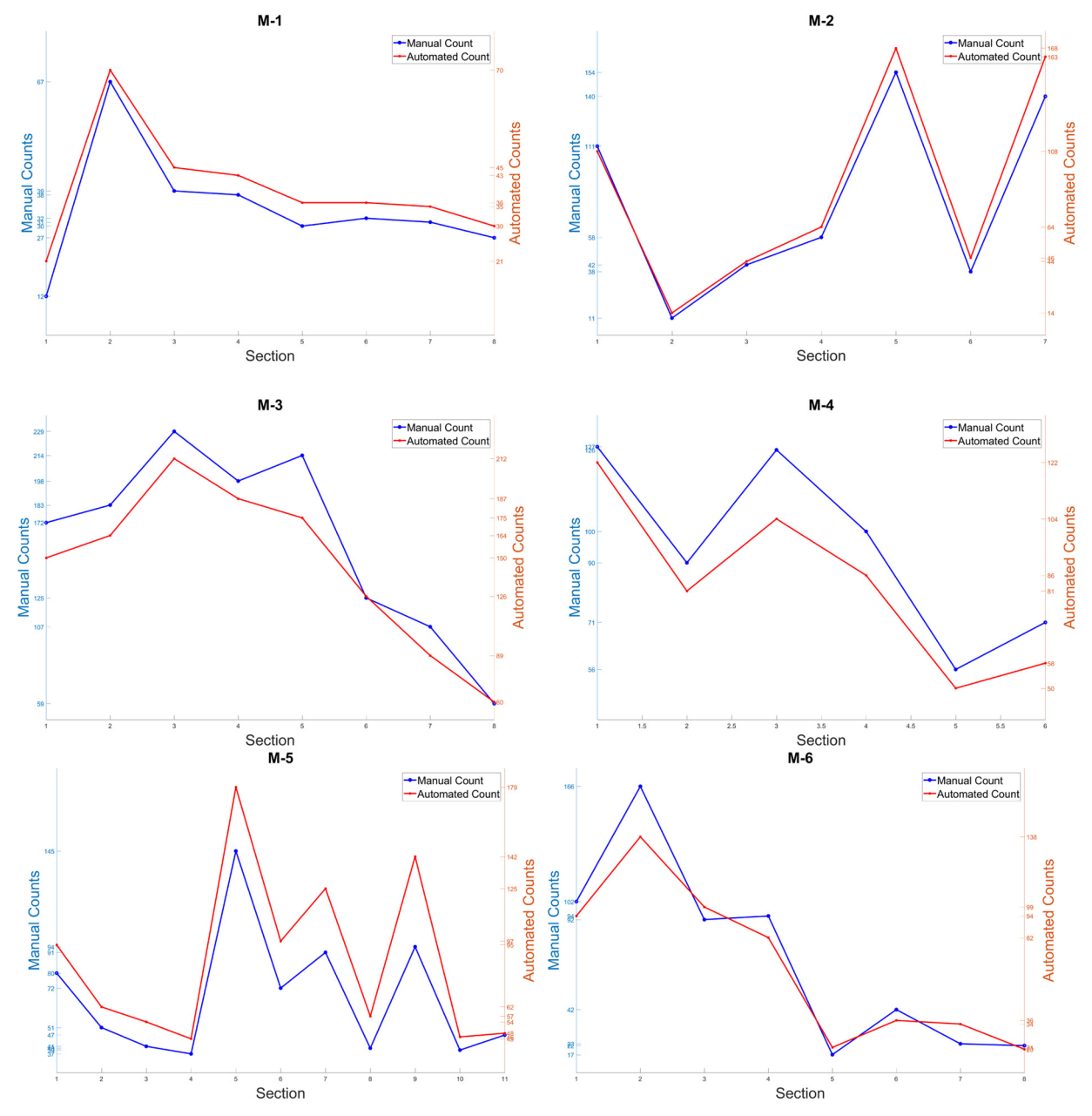


Fig. 3. Plots of manual and automated counts of different sections for six cases. These plots of NeuN neuron counts by section show the relative agreement between the objective automated framework and subjective manual counts.

below). A deep discussion of parameter changes for this work (to count Iba1-immunostained microglia cells) is done in Section 4.2.

3.3.2. Preprocessing

The image was preprocessed by the morphological operations opening by re-construction followed by closing by re-construction. These operations smooth the image and remove very small dark or bright regions (Fig. 2(d)). In this preprocessing step, very close regions were connected to each other and very small regional minimas were removed.

3.3.3. Foreground and background markers

After preprocessing the image foreground and background markers are extracted for watershed segmentation. The foreground markers are regional minimas extracted from the preprocessed image (Fig. 2(e)) and background markers are the boundaries between regions of a watershed segmentation (Fig. 2(f)). Regional minimas are an indication of neurons

and eventually those that do not fall into the previously segmented neuron clump regions were removed by reconstructing the regional minima map using the clumps map. Moreover, regional minimas with area smaller than a predetermined size, m_A , were removed.

3.3.4. Watershed segmentation

Watershed segmentation was applied using the foreground and background markers described in the previous step. One of the regions corresponded to the background and the others are foreground regions. Those foreground regions that overlap with the map of segmented clumps were kept and the others were discarded (Fig. 2(g)). This watershed segmentation usually expands original regional minimas and gives a better approximation of neuron boundaries. Lastly, each of the clump regions were split using the Voronoi diagrams obtained by the watershed regions inside it (Fig. 2(h)).

3.3.5. Boundary smoothing and neuron counting

In the final step, the region boundaries were refined using the Savitzky–Golay filter (Savitzky and Golay, 1964). This filter results in more smooth boundaries and produces less concave regions. It was observed that a single neuron or microglia cell may be split into two or more sub-regions if more than one regional minima was detected. To diminish the adverse effect of such splits, a region was not split if its size was less than a maximum threshold and the solidity of the region obtained by the refined boundary of the original region was larger than the average solidity of all regions obtained by the refined boundaries of sub-regions. To count the cells, those segmented regions that do not fall inside the disector frame or overlap with the exclusion line were removed and the number of the remaining regions were chosen as the number of counted cells for that disector location.

4. Experiments and results

The ASA approach was initially designed for automatic counts of NeuN stained neurons in images (Mouton et al., 2017). To evaluate the adaptability of this framework, this work applied ASA with minor modifications (discussed in Section 4.2) to detect and count Iba1-immunostained microglia cells. Other than the counts, we also report the correlation (in terms of \mathbb{R}^2) between the manual and automated counts for NeuN images to measure the effectiveness of the automation; and use precision and recall to measure the detection accuracy for automatic counts of Iba1-positive microglia. In these experiments, the performance of the framework was evaluated on one mouse, a few values for parameters were checked and set based on the obtained results and then the framework was tested on the remaining mice.

4.1. ASA for counts of NeuN and Iba1 images

We used the ASA to automatically count neurons in all cases. The offset f, introduced in Section 3.3.1, was set to 20. This offset was used due to the higher signal to noise ratio for NeuN and Iba1 images. Moreover, the minimum clump size, c_A (discussed in Section 3.3.1), was set to 1000 pixels. The correlation between the manual and automated counts were assessed by the R^2 measure at the section level. Therefore, for each section of a case the manual counts of all stacks were summed up to give the counts for that section of neurons (Fig. 3) and microglia (Fig. 4). Finally, the automated count is computed for each section and for the entire neocortex using the optical fractionator method. Table 1 presents the final manual and automated counts (the sum of all section counts) for different cases and the correlation between the manual and automated neuron counts at the section level. The estimates of the total number of neurons after application of the optical fractionator scheme can be obtained by extrapolating the raw data to the total neocortex. Finally, Fig. 3 presents the plots of the manual and automated counts for each of the NeuN cases.

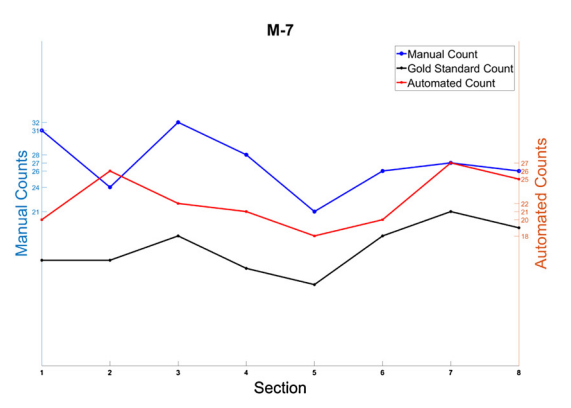


Table 1

Total manual and automated neuron counts of different cases in the dataset.

The counts represent the raw data for cells (neurons) sampled and counted through the entire neocortex in an unbiased systematic-random manner using the unbiased optical disector method.

Case	Manual count	Auto. count	R^2
M-1	276	316	0.99
M-2	554	607	0.99
M-3	1287	1163	0.96
M-4	570	501	0.95
M-5	737	950	0.96
M-6	558	524	0.97

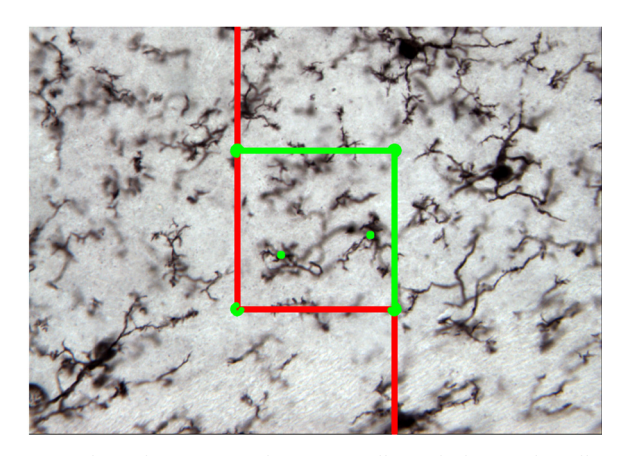


Fig. 5. Sample an Iba1 image with two manually marked microglia cells. Such images were manually annotated by a moderately-experienced data collector to create the manual truth for cell annotations.

4.2. Extension to other brain histology images

To evaluate the generalizability of the ASA approach to images stained for other proteins, we used the NeuN framework to automate the tasks of counting microglia cells in images from Iba1-immunoistained sections (Fig. 5). Because of the different characteristics of such images (e.g., contrast) and difference in size and appearance of microglia cells compared to neurons, modifications were needed in parameters trained for NeuN images, as discussed below. To assess the performance, Iba1 images from two cases, denoted by M-7 and M-8, were processed manually and the manual counts were compared to the automated counts achieved by the ASA. For this task, algorithm parameters were modified to achieve acceptable results on M-7 and the method with the new parameters were tested on M-8.

4.2.1. Microglia cell counting in Iba1 images

Segmenting microglia cells in Iba1 images is a relatively more

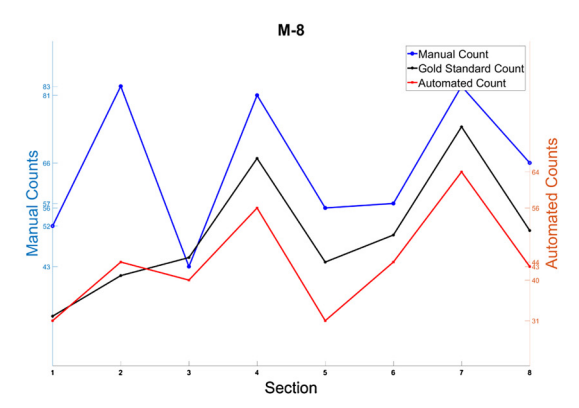


Fig. 4. Plots of manual truth, automated and gold standard counts of each section in Iba1 cases.

difficult task than segmenting neurons in NeuN images due to the presence of microglial processes (see Fig. 5). The ASA method for NeuN neurons was modified to also achieve acceptable results for Iba1 images. Three modifications that were applied to the step of *Clump Segmentation* (discussed in Section 3.3.1) are listed below:

- 1 Minimum clump size was decreased from 1000 to 900: because of the smaller size of microglia cells compared to neurons.
- 2 The structuring element used in morphological operations was enlarged from a radius of 5 to radius of 10: to remove microglial projections in the final segmentation.
- 3 The offset *f*, introduced in Section 3.3.1, was set to 70: because of the higher S:N ratio in Iba1 images compared to NeuN images.

Otherwise, all other steps of the ASA were used without modification. During the assessment of the quality of the annotation in the training dataset, it was observed that the counts were not accurate for some stacks of images. Therefore, an expert neurohistologist (PRM) recounted the microglia cells in all collected stacks. Hence, the microglia cells were counted in eight sections of each of two Iba1 cases both by a moderately experienced data collector (resulting in *Manual Truth*) and the expert (resulting in *Gold Standard*). Table 2 presents the manual truth, automated and gold standard counts for both cases used in this study. Moreover, to evaluate and compare the detection accuracy of the framework to that of the data collector, we present the detection measures, precision, recall and F1 score (Table 3).

Plots in Fig. 4 show the manual truth, gold standard and automated counts for each section of two cases in the Iba1 dataset. Table 3 presents the precision, recall and F1 score of the manual truth and automated method evaluated using the gold standard counts as the reference:

$$\begin{split} Precision &= \frac{TP}{TP + FP}, \quad Recall = \frac{TP}{TP + FN}, \\ F1Score &= 2 \cdot \frac{Precision \cdot Recall}{Precision + Recall}, \end{split}$$

where *TP*, *FP* and *FN* are True Positive (segmented cells that have an annotation in the gold standard dataset), False Positive (segmented cells that include no annotation) and False Negative (annotations that do not fall inside a segmented cell), respectively.

5. Discussion

The high correlation values between manual and automated counts of NeuN cases indicate that the framework can be used to automate the time-consuming and error-prone manual method for stereology counts of NeuN neurons images. With the exception of a few parameters such as minimum size of neuron regions (which was set based on image resolution), most of the parameters in the framework were set according to the properties of each image. This makes the results of the framework more reliable under variable conditions of image acquisition. As an example, it was observed that some of the images in the dataset were collected under the condition of varying light intensity. Because intensity thresholds were set adaptively, automatically and separately by the estimated GMM for each image, the framework produced consistent image segmentation despite apparent differences in image brightness. Fig. 6 illustrates two images with extreme intensities and their corresponding segmentation results.

In the Iba1 dataset, one case was used for parameter tuning and the

Table 2Total manual truth, automated and gold standard microglia counts of the two Iba1 cases.

Case	Manual truth count	Automated count	Gold standard count
M-7	215	179	132
M-8	521	353	404

Table 3Detection accuracy of microglia cells in terms of Precision, Recall and F1 Score of the manual truth and automated methods (superior results in each case are shown in bold text).

Case	Count	Precision	Recall	F1 score
M-7	Manual truth	59.53%	96.97%	73.77%
M-8	Automated Manual truth	70.39% 69.67%	95.45% 89.85%	81.03 % 78.48%
	Automated	96.32%	84.16%	89.83%

other case was used for testing. Initially, detecting microglia cells in Iba1 images was thought to be a relatively more challenging task than detecting neurons in NeuN images. After visually inspecting the results of ASA along with the data collector manual annotation (manual truth) for microglia cells counts in the first Iba1 case, it was found that the manual count and the automated count data were not in agreement in several cases; furthermore, this careful examination showed the ASA to be more accurate. Therefore, an expert neurohistologist was asked to manually review and count microglia cells in all the stacks, resulting in the Gold Standard dataset that contained the fewest errors. In the final analysis, the manual truth and automated counts created by the ASA were checked against the gold standard counts manually and the detection accuracy was quantified. As summarized in Table 3, the automated count had higher overall detection accuracy for both cases examined, achieving about 10% higher accuracy in terms of F1 score than manual truth counts.

Through careful investigation of these results we identified three sources of segmentation errors in NeuN and Iba1 counts using the ASA-optical fractionator framework: (1) very high density cell populations; (2) cells with very low contrast (low S:N); and (3) image artifacts. The errors caused by artifacts or cells with very low contrast can be potentially minimized by extra preprocessing steps to remove artifacts and post-processing steps to merge over-segmented regions. Complete elimination of segmentation errors for high density cell populations is a more challenging task that we are addressing with ongoing studies involving 3D segmentation, iterative neural networks and active deep learning. Fortunately, very high density populations are rare events for the vast majority of cells, including NeuN neurons and Iba1 microglia cells in brain tissue.

Testing is ongoing using ASA to create segmentation ground truth for training a CNN to further reduce the error rates and increase the robustness of the whole framework for automatic counting of multiple populations of immunostained cells on tissue sections. Finally, future work will explore the tolerance of this approach under variable conditions of low to high S:N, staining protocols and biological structures.

6. Conclusions

These experiments with new image datasets expand our previous work with a small set of NeuN (neurons) images to show that the ASA-optical fractionator framework can be successful with a range of staining domains from multiple types of immunostained brain cells. The results for NeuN counting confirm earlier reports of high correlation with manual annotation (with $R^2 > 0.95$). Testing with Iba1 microglia cell slides to get counts showed the ASA-optical fractionator framework is substantially more accurate than a moderately experienced data collector when compared to the results of an expert neurohistologist. Moreover, Iba1 microglia cells showed lower error rates than for NeuN neurons, most likely due to less cell overlap for Iba1 microglia than NeuN neurons in the mouse neocortex. Together, these results provide further indication that automatic stereology can reliably replace the manual, labor-intensive and tedious process of cell counting by a moderately experienced data collector with a method that decreases the

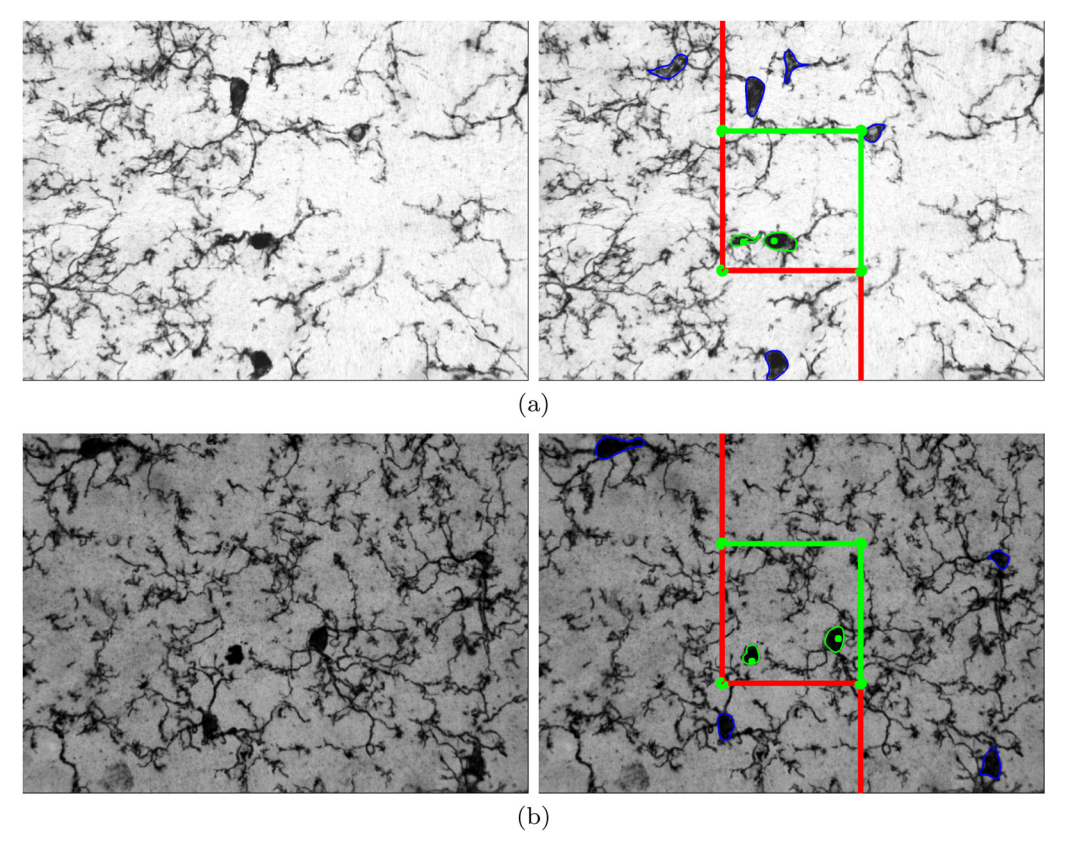


Fig. 6. Two EDF images with very different brightness levels and their segmentation results. This visual comparison shows how the method achieved consistent results under varying intensity as it could find and mark all cells in both images correctly.

time, effort and costs of stereology data collection while increasing the accuracy, precision and throughput of the final results. This attribute may be especially useful in settings where computer-assisted equipment is present but expert and highly trained data collectors are not available or are needed for more highly technical activities. Finally, these findings show that the ASA approach can be effectively used to automatically annotate EDF images of NeuN neurons and Iba1 microglia cells for automatic counts by deep learning neural networks.

In our ongoing work (Alahmari et al., 2018, 2019), this feature shows promising results for automatically generating segmentation ground truth datasets for training CNN models to make automatic stereology counts of brain cells. The segmentation ground truth generated by ASA is used to train an iterative deep learning segmentation model with human-in-the-loop to reject, verify or modify the segmentations. Using ASA to generate the initial ground truth segmentation masks significantly reduced the time needed for manual annotation and segmentation mask creation and hence made training a robust deep learning model practical.

Acknowledgements

All authors declare that this work is presented in the absence of any real or perceived conflict of interest. Author Peter R. Mouton, Ph.D., Chief Scientific Officer of SRC Biosciences (Tampa, Florida, USA) is the owner of Intellectual Property for the Stereologer system. Authors PRM, DG, LOH hold a U.S. patent on "Automatic stereological analysis of biological tissue including section thickness determination" (U.S. Patent 9297995) and have filed a number of related patent applications (WIPO Patent Application WO/2018/089783; U.S. Patent Application 20120236120), which may be related to products or product developments of SRC Biosciences Company, including the "Adaptive Segmentation Algorithm (ASA)" used for performing unsupervised (automatic) stereology as described in several co-authored papers

referenced in this work. For work described in this paper all authors have received grant support from a Small Business Innovative Research (SBIR) grant from the National Institutes of Health (NIH-MH076541) and Small Business Technology Transfer Research (STTR) grant (NSF#1746511) from the National Science Foundation (NSF).

References

Ahmady Phoulady, H., Goldgof, D., Hall, L.O., Mouton, P.R., 2017. A framework for nucleus and overlapping cytoplasm segmentation in cervical cytology extended depth of field and volume images. Comput. Med. Imag. Graph. 59, 38–49.

Alahmari, S., Goldgof, D., Hall, L., Dave, P., Ahmady Phoulady, H., Mouton, P., 2018. Iterative deep learning based unbiased stereology with human-in-the-loop. 2018 17th IEEE International Conference on Machine Learning and Applications (ICMLA), IEEE 665–670.

Alahmari, S.S., Goldgof, D., Hall, L., Phoulady, H.A., Patel, R.H., Mouton, P.R., 2019.
Automated cell counts on tissue sections by deep learning and unbiased stereology. J. Chem. Neuroanat. 96, 94–101.

Bradley, A.P., Bamford, P.C., 2004. A one-pass extended depth of field algorithm based on the over-complete discrete wavelet transform. Image and Vision Computing'04 New Zealand (IVCNZ'04) 279–284.

Gundersen, H.J.G., 1977. Notes on the estimation of the numerical density of arbitrary profiles: the edge effect. J. Microsc. 111 (2), 219–223.

Mouton, P.R., Ahmady Phoulady, H., Goldgof, D., Hall, L.O., Gordon, M., Morgan, D., 2017. Unbiased estimation of cell number using the automatic optical fractionator. J. Chem. Neuroanat. 80, A1–A8.

Mouton, P.R., 2002. Principles and Practices of Unbiased Stereology: An Introduction for Bioscientists. JHU Press.

Mouton, P.R., 2011. Unbiased Stereology: A Concise Guide. JHU Press.

Santacruz, K., Lewis, J., Spires, T., Paulson, J., Kotilinek, L., Ingelsson, M., Guimaraes, A., DeTure, M., Ramsden, M., McGowan, E., et al., 2005. Tau suppression in a neurodegenerative mouse model improves memory function. Science 309 (5733), 476–481.

Saper, C.B., 1996. Any way you cut it: a new journal policy for the use of unbiased counting methods. J. Comp. Neurol. 364 (1), 5.

Savitzky, A., Golay, M.J., 1964. Smoothing and differentiation of data by simplified least squares procedures. Anal. Chem. 36 (8), 1627–1639.

West, M., Slomianka, L., Gundersen, H.J.G., 1991. Unbiased stereological estimation of the total number of neurons in the subdivisions of the rat hippocampus using the optical fractionator. Anatom. Rec. 231 (4), 482–497.